ACS APPLIED MATERIALS & INTERFACES

Research Article

www.acsami.org

Tuning InAs Nanowire Density for HEK293 Cell Viability, Adhesion, and Morphology: Perspectives for Nanowire-Based Biosensors

Sara Bonde,[†] Trine Berthing,[†] Morten Hannibal Madsen,[‡] Tor Kristian Andersen,[†] Nina Buch-Månson,[†] Lei Guo,[†] Xiaomei Li,[†] Florent Badique,[§] Karine Anselme,[§] Jesper Nygård,[‡] and Karen L. Martinez*[,†]

[†]Bionanotechnology and Nanomedicine Laboratory, Department of Chemistry and Nano-science Center, University of Copenhagen, Universitetsparken 5, DK-2100, Copenhagen, Denmark

[‡]Nano-science Center and Center for Quantum Devices, Niels Bohr Institute, University of Copenhagen, Universitetsparken 5, DK-2100, Copenhagen, Denmark

[§]Institut de Science des Matériaux de Mulhouse (IS2M), CNRS UMR7361, Université de Haute-Alsace,15, rue Jean Starky, BP 2488, F-68057 Mulhouse cedex, France

Supporting Information

ABSTRACT: Arrays of nanowires (NWs) are currently being established as vehicles for molecule delivery and electrical- and fluorescence-based platforms in the development of biosensors. It is conceivable that NW-based biosensors can be optimized through increased understanding of how the nanotopography influences the interfaced biological material. Using state-of-the-art homogenous NW arrays allow for a systematic investigation of how the broad range of NW densities used by the community influences cells. Here it is demonstrated that indium arsenide NW arrays provide a cell-promoting surface, which affects both cell division and focal adhesion up-regulation. Furthermore, a systematic variation in NW spacing affects both the detailed cell morphology and adhesion properties, where the latter can be predicted based on changes in free-energy states using the proposed theoretical model. As the NW density influences cellular parameters, such as cell size and adhesion tightness, it will be important to take NW density into consideration in the continued development of NW-based platforms for cellular applications, such as molecule delivery and electrical measurements.

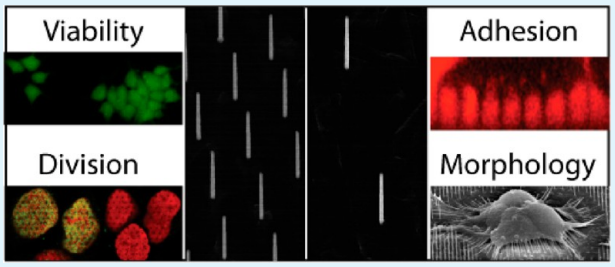

KEYWORDS: *nanopillar, nanorod, focal adhesion, nanowire spacing, nanotechnology, fluorescence, SEM, live cell imaging*

INTRODUCTION

Nanostructured surfaces are currently being developed for a variety of cellular applications, such as biosensors and smart materials.[1−4] Recently, arrays of vertical nanowires (NWs) have been demonstrated to have great potential for several interesting cellular applications, such as intracellular electrical measurements, molecule delivery, and fluorescence-based biosensing.[5−8] In this context, it is of great interest to understand how the nanotopography will influence the biological material it is interfaced with. Quantifying the effect of nanotopography on cellular responses is believed to alleviate further development of NW-based platforms, for example, to gain intracellular access or to form a tight seal for electrical measurements. However, previous studies have been conducted on various kinds of nanomaterials, or more importantly on arrays with random NW geometries, with only a single exception using regular NW arrays.[9]

Several parameters of NW geometry, such as NW length or diameter, could potentially affect cellular response. The scope of this paper is to tune the NW density across the wide range of NW spacings used in the community, while maintaining all other geometrical properties strictly constant. Whereas investigating the NW influence on cell fate will be key for any application, certain parameters will be more critical than others to better tune the geometry of NW arrays for each application. The hypothesis brought forward here is that NW density will influence the following four cellular parameters, key to biosensor development, namely: cell viability, adhesion, morphology, and division.

Cell viability has previously been partly studied, and cells have been shown to adhere spontaneously to arrays of vertical nanostructures of a broad variety of materials and dimensions.[10−16] The cell health is maintained up to several weeks on NW arrays, and has previously been investigated mainly in terms of descriptive cell morphology and viability.

Cell adhesion is mediated through dynamic signaling complexes called focal adhesions (FAs).[17−19] They are composed of a plethora of intra- and extracellular proteins such as vinculin and paxillin, which link the actin cytoskeleton to the extracellular matrix. Their presence on arrays of NWs has

Received: May 30, 2013
Accepted: September 27, 2013
Published: September 27, 2013

been noted previously.[20] Furthermore, the adhesion tightness between NW chip surface and cells is believed to be crucial for biosensor development.[6,7,21] The shift between loose and tight adhesion has previously been suggested to depend on a critical distance between NWs, above which cells can no longer reach between and stay on top of the NWs, and thus settle down tightly into the structure.[9] Moreover, since NWs do not systematically penetrate the plasma membrane,[13,22] it is plausible that the energy required to form tight membrane invaginations around NWs will also impact the adhesion tightness.

Cell morphology on arrays of NWs has most commonly been referred to in qualitative terms. Quantitatively, parameters such as cell area and aspect ratio can be extracted by utilizing algorithms to characterize cell size and shape. This allows for objective and detailed investigations of cell morphology that few studies with cells on vertical NWs have taken advantage of so far.[9,23−26]

Finally, cell division involves the synthesis of new DNA, formation of mitotic spindles, and finally division into daughter cells.[27] Cell division has previously been shown to occur on arrays of NWs.[28] Subdividing the cell division event into three key cell cycle phases (S-, M-, and cytokinesis phase) allows for detailed investigation of the synthesis of DNA, formation of mitotic spindles, and completed cytokinetic cell division on arrays of NWs. In particular, it can be investigated how cell division is affected by the presence of a range of NW densities.

Owing to recent advances in nanotechnology, high-aspect-ratio NWs can now with high reproducibility be grown to precise lengths and diameters, and importantly be positioned at fixed distances from each other. In this study we take advantage of chips with arrays of vertical indium arsenide (InAs) NWs with a precisely controlled geometrical design, attained only by few others. We investigate, in large cell samples and with reduced data discrepancies, how detailed cell viability, morphology, adhesion, and division are affected by a systematic variation of the distance between NWs. The HEK293 cells have been chosen for this study as it is one of the major cell lines in drug screening,[29,30] and is currently used as a model system in the development of nanoscale sensors.[7,11] By screening a broad range of NW densities and spacings, the results obtained are believed to be generically applicable to a majority of the NW arrays developed so far, and considerably alleviate the further development of NW arrays for cellular applications.

MATERIAL AND METHODS

Fabrication of InAs NW Arrays and Control Surface. The Au catalyst droplets were positioned with electron beam lithography in homogeneous arrays with 2, 3, 5, 7, and 10-μm spacing. InAs NWs were grown through Au-assisted vapour-liquid-solid growth mechanism using molecular beam epitaxy as previously described.[22,31] For further details of NW growth, see the Supporting Information. Each multidensity chip growth was characterized for mean NW diameter and length using scanning electron microscopy (SEM; JEOL JSM-6320F). On the control surface, no Au droplets were added, thus producing a flat surface with only a slight roughness created by the overall growth process (Figure S1, Supporting Information).

Measurement of Surface Roughness. For measuring the surface roughness, atomic force microscope images were obtained using a Park NX20 microscope run in intermittent mode with a scan frequency of 0.1 Hz. Two areas were imaged on the NW chips; one area 100 μm from the NW arrays, and one area in between NWs with a pitch of 10 μm. All imaged areas were at least 5×5 μm^2. Data was analyzed in the SPIP software, where a line-wise fit correction was applied prior to surface roughness analysis.

Culturing and Interfacing Cells with NW Chips. HEK293 cells (Sigma) and HEK293 cells transformed with a fluorescent protein fused to a lipid anchor (N_Gi-a2-Citrine-C_G-g2) (HEK293-citrine)[32] were maintained at 37°C, 5% CO_2, and >95% humidity in DMEM/F-12 Glutamax-I medium with 10% fetal bovine serum, as previously described.[22] The HEK293-citrine cells were cultured in the presence of geneticin/G-418 (400 μg/mL). The InAs NW chips were sterilized in ethanol, washed in Milli-Q water, and interfaced with suspended cells in DMEM with 10% FBS and penicillin-streptomycin. 20−80 000 HEK293 cells/cm^2 were drop-wise added to the NW chips and flame sterilized glass coverslips. In all experiments, cells were cultured for 48 h before investigations.

SEM Imaging. For SEM imaging, cells were washed in phosphate buffered saline (PBS, Gibco Invitrogen) and incubated in 2% glutaraldehyde in PBS. The sample was dehydrated in increasing concentrations of methanol, air-dried, and sputter coated with 5 nm Au.

Live-Cell Labeling. For live-cell imaging of cell morphology and viability, cells were labeled with 3 μM calcein-acetoxymethyl (AM), 6 μM ethidiumhomodimer-1 (EthD-1) (both Invitrogen), and 5 μM DRAQ5 (Biostatus). Samples were imaged using an upright wide-field fluorescence microscope (Leica DM5500 B). NWs were visualized using either differential interference contrast or dark field imaging.

Cell Morphology. The cell morphology in terms of cell area and aspect ratio (the ratio between the longest and shortest diameter of the cell) was quantified. Using CellProfiler software (version 2.0, Massachusetts Institute of Technology, Cambridge, MA), all nuclei were identified based on the DRAQ5 nuclear images. A propagation method was used to find the boundaries of each cell in the corresponding calcein-AM cytosol images.

BrdU Labeling. Cells were incubated with 0.03 mg/mL of the thymidine analogue bromodeoxyuridine (BrdU, Invitrogen) in DMEM with 10% FBS for 5 h, before the cells were rinsed in PBS and fixed in 4 % paraformaldehyde (PFA) for 30 minutes. Samples were thereafter rinsed and incubated for 1 h in 1.5 M HCl to expose the incorporated BrdU.

Immunocytochemistry. For immunocytochemistry, cells were rinsed in PBS, incubated in 4% PFA for >10 minutes, and rinsed in PBS, before pre-incubation in blocking solution (0.25% Triton-X in PBS with 5-10% normal rabbit serum) for 1 h. Samples were thereafter incubated with either of the primary antibodies: anti-tubulin (2.5 μg/mL, Sigma), anti-BrdU (2 μg/mL, Invitrogen), or anti-vinculin (5 μg/mL, Sigma) (all raised in mouse). Samples were thereafter rinsed in blocking solution, followed by incubation in either of the secondary antibodies: biotinylated rabbit-anti-mouse (1:200, Sigma, for tubulin) or rabbit-anti-mouse-Alexa488 (1 μg/mL, Invitrogen, for vinculin and BrdU). The anti-tubulin sample was rinsed in 0.25% Triton-X in PBS and incubated in Alexa488-conjugated streptavidin (2 mg/mL, Invitrogen). The BrdU-labeled samples were counterstained with DRAQ5 and imaged using a Leica DM5500 B upright wide-field fluorescence microscope. All other samples were imaged with a Leica TCS SP5 confocal microscope.

For actin labeling, the fixed sample was permeabilized with 0.2% Triton-X, pre-incubated with 1% BSA in PBS, before being stained with rhodamine-phalloidin (2%, Invitrogen).

Cell Cytokinesis. For time-lapse measurements of live cell cytokinesis, a Zeiss LSM700 confocal microscope with environmental control (CO_2, humidity, temperature) was used to sample images of HEK293-citrine cells every 5 min for 13 h.

Cell Detachment. Allowing suspended cells to adhere to a surface, and thereafter by rinsing to discard the nonattached cells, has been the standard approach to measure cell adhesion for the past decades.[33] Here the classical rinsing assay has been further improved by imaging the full area of the chips with overlapping frames both before *and* after rinsing the sample 1, 3, 10, 20, and 30 times with 150 μL of DMEM with HEPES. The multidensity chips were washed in different orientations in a random manner to guarantee homogenous rinsing across each sample. The number of cells was counted based on the labeled nuclei using CellProfiler.

Focal Adhesion Density, Area, and Shape. Focal adhesions (FAs) were analyzed through a combination of ImageJ (version 1.47b, National Institutes of Health, Bethesda, MD) and CellProfiler software. Image stacks were collected by confocal imaging, the bottom 2 μm of the stack were summed, a constant threshold was applied, and the image was converted to a mask of FAs using ImageJ. The whole stack was summed to identify cell outlines and nuclei, and the slice covering the gold tip reflection was used to identify the position of the NWs. CellProfiler was then used to analyze FA position, density, area, and shape. The FA density is the number of FAs per 100 μm^2, and FA form factor is calculated as $4\pi \times$ area/perimeter^2, which for a perfectly circular object equals 1, and 0 for a line. FAs smaller than 0.1 μm^2 were filtered out.

Cell–NW Proximity. For imaging the live-cell proximity to the NW chip surface, the sample was immersed in calcein-AM and 100 μM ATTO647, and image stacks were collected on a Leica TCS SP5 confocal microscope. The distance between the apical side of the cell and the NW array surface was measured using resliced side-views of the image stacks in ImageJ software.

Statistics. All data was compared using Student's unpaired *t* test, with a two-tailed distribution. A *p*-value below 0.05 is considered a significant difference. All experiments are performed at least in triplicate samples, and results are presented as mean value ± standard error of the mean, unless otherwise noted.

RESULTS

Cell Growth on Highly Ordered Arrays of Vertical NWs. To perform systematic studies regarding cell behavior on NW arrays of various densities, we chose to design a multidensity chip containing all the NW densities to be tested, as well as the control surface. This allowed for gathering all the data from single chips, and thus minimizing sample discrepancies and reducing data discrepancies. Arrays of vertical NWs were precisely manufactured in 500 × 500 μm^2 regions with 2, 3, 5, 7, and 10 μm spaced NWs (center-to-center), corresponding to a NW density of 29, 13, 5, 2, and 1 NW/100 μm^2, respectively (Figure 1A). The NWs on these multidensity chips were grown to a height of 4.4 ± 0.3 μm, with a diameter of 92 ± 6 nm (mean ± standard deviation, $n > 30$ NWs), unless otherwise noted. The reproducibility of the manufacturing method is apparent from the low standard deviation, and visualized using SEM (Figure 1B), and importantly allows us to keep the NW length and diameter strictly constant and exclude their influence on the observed cellular responses. The surface next to the NW arrays was used as a control, since the surface roughness here is the same as the surface roughness between the NWs (S_a/S_q = 20/25 nm and S_a/S_q = 14/19 nm, respectively; Figure S1, Supporting Information). Throughout this report, we will consistently refer to *both* NW spacing and density.

To investigate how the cell–NW interface is affected by a systematic variation of NW density, HEK293 cells were gently interfaced with NW chips (Figure 1C–E). Cells are present on all densities to a similar extent (Figure 1D), and it is striking that the NW density affects the morphology of the cells. On the highest NW density (29 NWs/100 μm^2 = 2 μm spacing), the cells appear rounded and smaller, whereas on the lower densities the cells seem to spread out more and cover a larger area of the NW array (Figure 1C).

Tuning Cell Morphology by Varying NW Density. To confirm the qualitative cell-morphology finding, and to make sure this is not an artifact of the SEM preparation, the morphology of living cells was investigated using algorithms for cell area and aspect ratio. In line with our qualitative results from the SEM images, this detailed investigation shows that cell

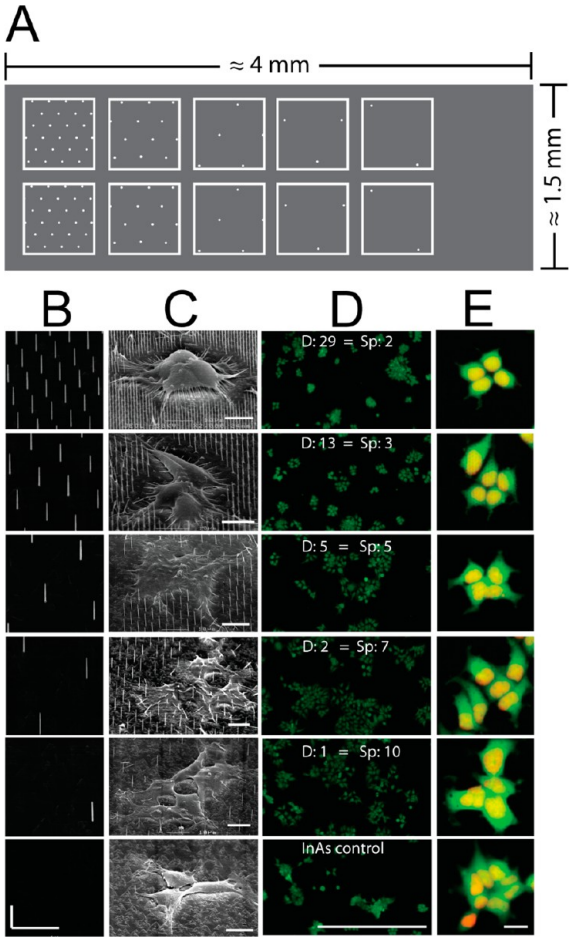

Figure 1. Cell growth on highly ordered arrays of vertical InAs NWs. (A) Schematic layout of the multidensity chip with 500 × 500 μm^2 arrays (white squares) of vertical NWs with either 2, 3, 5, 7, or 10 um spacing between wires, corresponding to 29, 13, 5, 2, 1 NW/100 μm^2, respectively. On the same chip, next to the arrays, is flat InAs used as control surface. (B) NW samples were imaged using SEM at a 17° tilt showing the homogeneity in pitch, length (4.4 μm), and diameter (92 nm). (C) HEK293 cells were grown for 48 h on the NW chips and appear to adapt with a smaller, more rounded morphology on high-density array of 29 NWs/100μm^2, and a more flat and spread-out morphology on the lower densities. (D, E) Living cells show maintained esterase activity (green = calcein-AM) while interfaced with the NWs, and the morphology of the cells appears qualitatively similar in wide-field microscopy (red = DRAQ5 nuclear label). Sp = spacing, D = density. Scale bar A = 5 μm, B = 10 μm, C = 500 μm, D = 20 μm.

area increases as the NW density decreases ($n > 500$ cells per surface) (Figure 2A). On the low-to-mid densities (1, 2, 5 NWs/100μm^2) the cells have a significantly larger area as compared to the highest NW density and InAs control. Compared to glass control, the cell area is significantly larger on the lowest density, and significantly smaller on the highest density. The cell aspect ratio shows that cells are significantly more elongated on the low-density array, as compared to the high-density NW array and InAs control (Figure 2B). In summary, this shows that a low NW density, of just a few NWs per cell, promotes cells to spread out and have a larger area and higher aspect ratio than on controls.

A Wide Range of NW Densities Does Not Affect Cell Viability. To evaluate which NW density will be the most appropriate for different types of biosensors, it is of crucial

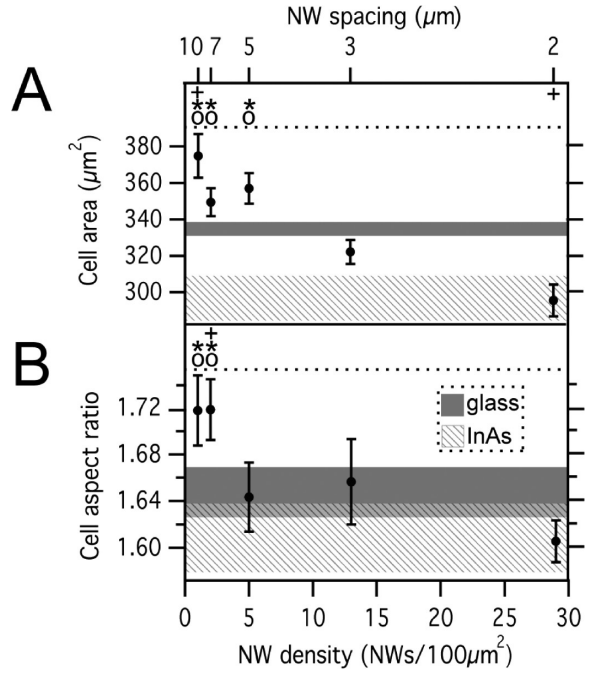

Figure 2. Tuning cell morphology by varying NW density. The morphology of the living cells (calcein-AM) adapts quantitatively to the pitch between NWs, where (A) the cell area is significantly increased on low-density arrays compared to the InAs (∗) and glass (+) controls, and high-density array 29 NWs/100 μm^2 = 2 μm spacing (○). The area on the high-density array is significantly smaller than on glass coverslip (+). (B) The cells elongate more and have a significantly higher aspect ratio on the low-density arrays as compared to the InAs (∗) and glass (+) controls, and the high-density array (○). Values are compared to glass (solid gray) and InAs (striped gray) control surfaces, ± standard error of the mean.

importance to evaluate different aspects of the cell health on the NW densities. Thus, the cell membrane integrity and the cell esterase activity were investigated on the different NW densities. We find that these two parameters of cell health are not affected by the presence of NWs in the density range tested here. The cell viability is maintained over 95%, which is similar to controls (n > 800 cells per surface) (Figure 3).

Cell Division on NW Arrays. To further evaluate the cell fate on arrays of NWs, the cell division was investigated in detail by observing progression through three phases of the cell

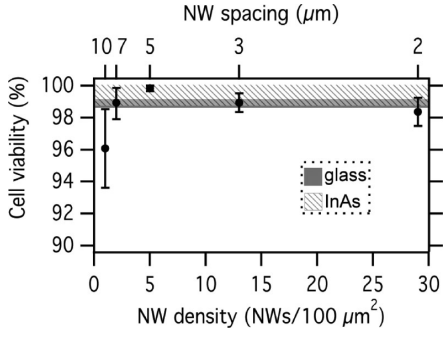

Figure 3. A wide range of NW densities does not affect cell viability. Irrespective of the NW spacing, the cell esterase activity (calcein-AM) and cell membrane integrity (ethidium homodimer-1) is maintained above 95%. Values are compared to glass (solid gray) and InAs (striped gray) control surfaces, ± standard error of the mean.

cycle. Firstly, DNA synthesis was evaluated by incubating the cells with the thymidine analogue BrdU (Figure 4A). BrdU is incorporated into DNA during the S-phase of the cell cycle, and is detected in cells via subsequent immunocytochemical labeling of its bromo-epitope.[34] Interestingly, this investigation demonstrates that the number of BrdU+ cells is increased on the NWs as compared to controls (n > 900 cells per surface) (Figure 4B).

Secondly, the labeling of the tubulin cytoskeleton confirmed that cells on all NW densities can successfully form mitotic spindles, which are characteristic of the M-phase of the cell cycle (Figure 4C). The orientation of the mitotic spindle is not biased by the presence of vertical NWs, where all between parallel and perpendicular spindles were observed (data not shown).

Finally, to investigate if cells on the NWs can progress through the cell cycle cytokinesis and form two daughter cells, HEK293 cells stably expressing a membrane anchored protein labeled with citrine were interfaced with the NW chips. Using time-lapse imaging, it is demonstrated with direct proof that cells can divide on NWs (Figure 4D; Supporting Information Movie S1). The first cell division takes place already within 1 h after plating the cells, and the whole process lasts about 1 h. During cytokinesis the cell lifts itself off the surface, goes out of focus from the confocal z-plane, and after completed cell division returns down to the surface again. The time-lapse imaging also demonstrates the dynamic nature of the cells on NW arrays, revealing a rapid extension and retraction of cellular processes (Movie S1, Supporting Information). Intriguingly, when cells are settled on the NWs, the nuclear membrane is pushed up to an extreme curvature around each NW (Figure S2, Supporting Information). Taken together, these findings show that the presence of NWs influences cell division, by increasing the number of cells in the S-phase and allowing cells to proceed through M- and cytokinesis phases of the cell cycle, despite an extreme deformation of the nuclear membrane.

NWs Reduce the Level of Cell Detachment. Highly relevant for the design of NW-based biosensors, is to investigate the adhesion profile of cells. Firstly, the detachment of cells from NW arrays and controls were evaluated by performing a rinsing assay (Figure 5). By the third rinse, the percentage of remaining cells was already greatly reduced for the controls, with 73% cells remaining on the InAs control and only 25% on the glass control. By rinse 10, almost all the cells were gone on the glass control. The percentage of remaining cells on the InAs control had continued to drop by the 10th and 20th rinse, and only 24% of the cells remained by rinse 30. In contrast, about 80% of the cells still remained adhered to the NW arrays (n > 1500 cells initially per surface). Through this test, it was clearly established that cell detachment is reduced on the NW arrays as compared to controls.

Cell–NW Adhesion Involves the Cytoskeleton and Focal Adhesion Formation. To investigate how the cells are able to adhere stronger to the NWs, the actin cytoskeleton was labeled. In controls, the HEK293 cytoskeleton remains diffuse across the cell cytoplasm (Figure S3, Supporting Information). On NWs however, it is clear that the actin-rich extremities of the cells almost always colocalize with NWs (Figure 6A), demonstrating a prevalent interaction between the NWs and cell cytoskeleton. Stabilization of the actin cytoskeleton around NWs along the cell edges could contribute to the increased cell adhesion through a physical entrapment of the cells.

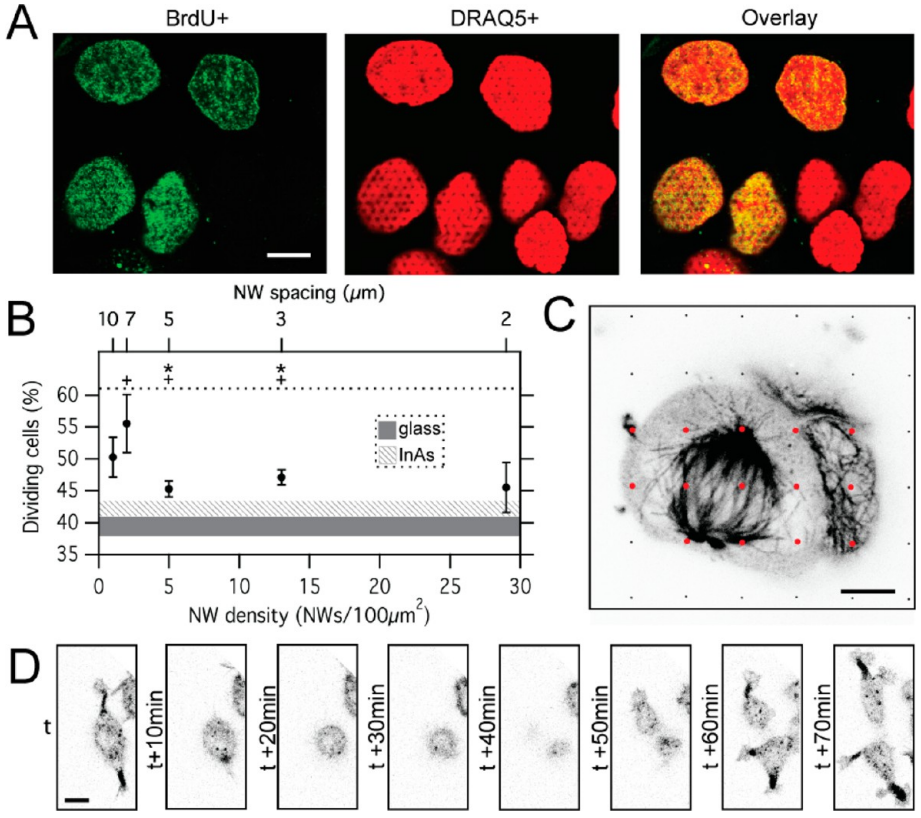

Figure 4. Cell division on NW arrays. (A) By labeling newly synthesized DNA with the thymidine-analogue BrdU (green), it is demonstrated that cells (nuclei, red) undergo the cell cycle S-phase on NW chips. NWs can be seen as regular dark shadows in the nuclei. (B) The number of BrdU+ cells on the NW arrays is significantly increased compared to glass (+) and InAs (∗) controls, and a tendency for some densities to be different than others. Values are compared to glass (solid gray) and InAs (striped gray) control surfaces, ± standard error of the mean. (C) CelIs undergo the cell cycle M-phase on all NW densities. Presented is an example of a cell labeled with anti-tubulin cytoskeleton on 10 um long NWs on the mid-density array (5 NWs/100μm^2 = 5 μm spacing). NWs are drawn into the image (gray dots) and emphasized across the cell (red dots). (D) Finally, it is demonstrated that cells proceed all the way through the cell cycle and undergo cytokinesis by dividing into two progeny cells on the mid-density array over the course of 1 h, already within 1 h after plating. Cells are labeled through constitutive expression of membrane-anchored citrine (HEK293-citrine). Scale bar A = 10 μm, C = 5 μm, D = 10 μm.

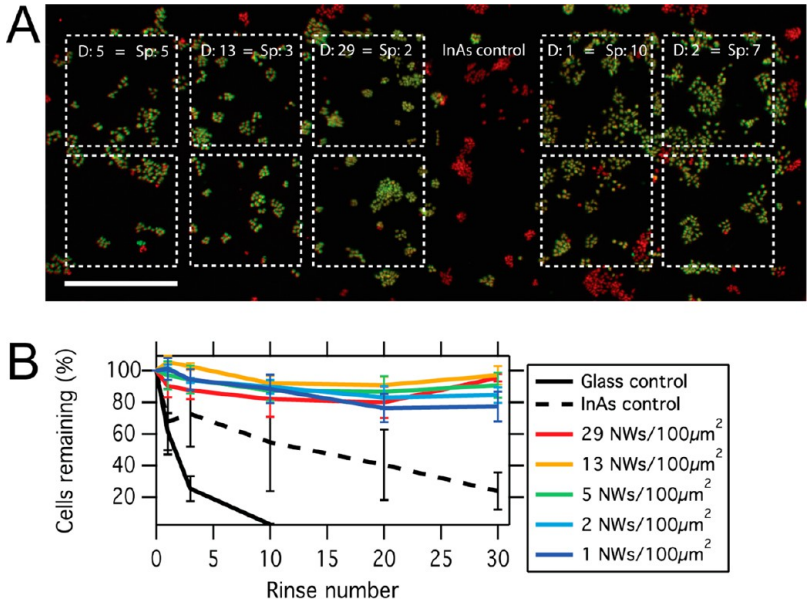

Figure 5. NWs reduce cell detachment. (A) Cells growing on the NW chips were labeled and exposed to a rinsing assay. All cells still remaining after rinse 30 are false-colored green, and all cells removed by rinse 30 are false-colored red, demonstrating that cells adhere better to the NW arrays than to the flat InAs. D = density (NW/100μm^2), Sp = spacing (μm). Scale bar = 500 μm. (B) The percentage of remaining cells is normalized to initial cell number, showing that cells on control surfaces, InAs, and especially on glass coverslip adhere to a lesser extent than cells on the NW arrays.

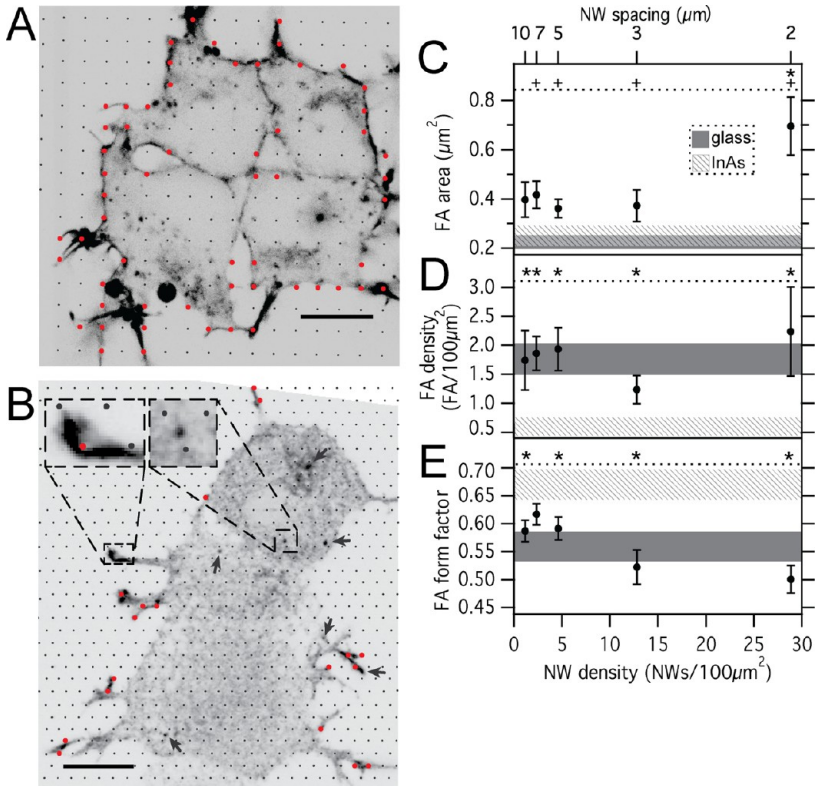

Figure 6. Cell−NW adhesion involves the cytoskeleton (A) and FA formation (B−E). (A) The square-patterned NWs (gray/red dots) contribute to the adhesion and the shape of the cells by dictating the adhesion of the cell edges. The actin-rich (rhodamine-phalloidin, black) cell edges and cell processes almost always colocalize with NWs (red dots). NWs are 10 μm long. (B) The position of FAs is not preferentially associated with NWs, but both colocalize (red dots and left inset) and do not colocalize (arrows and right inset) with the NWs. (C) The size of FAs is significantly larger in cells on NWs as compared to glass (+) and InAs (∗) controls. (D) The FA density is significantly increased in cells on NWs as compared to InAs control (∗). (E) The FA form factor is significantly smaller in cells on NWs as compared to InAs control (∗). (A, B) The NWs were drawn into the actin and FA images based on the NW reflection image. Scale bars = 10 μm. (C−E) Values are compared to glass (solid gray) and InAs (striped gray) control surfaces, ± standard error of the mean.

FAs are localized areas of connection between the cells and the extracellular matrix (here: NW chip). FAs are also points of intracellular signaling, mediated e.g. through the actin cytoskeleton. To investigate if FAs, like the actin cytoskeleton, are strongly associated with the NWs, FA position, density and morphology were investigated. We find that FAs are not predominately localized to the NWs, but are also formed in the space between the NWs on all densities; from high-density (Figure 6B) to low-density arrays (Figure S4, Supporting Information). Interestingly though, the FA area is significantly increased in cells on NWs as compared to especially glass control (n > 50 FAs per surface) (Figure 6C). Furthermore, the density of FAs was increased on NWs (Figure 6D), and the morphology of FAs was altered to exhibit more elongated FAs (reduced form factor value) in cells interfaced with NW arrays as compared to the InAs control (Figure 6E) (n = 15−26 cells per surface). In summary, this shows that the stronger cell adhesion on the NW arrays could be explained by a combination of actin-dependent physical entrapment and upregulated FA formation.

Tuning and Predicting the Density-Dependent Proximity between Cells and NWs. To tune the tightness between the cells and the NW chip surfaces is of great importance for the development of biosensors, for example, to get a good electrical seal.[6,7,21] Therefore, it was investigated how closely the cells adhere to the surface of the NW chip, by using a small molecular dye in the extracellular fluid around living cells. Here it is clearly demonstrated that cells on high-density arrays are rather "floating" on the NW tips, whereas cells on the low-density arrays form adhesion "footprints" on the NW chip surface, by adhering all the way down the length of the NWs (Figure 7A). The distance between cells and the NW chip surface is significantly dependent on the NW density, where a lower NW density entails a reduced distance between cells and the NW array surface (n > 30 cells per NW density) (Figure 7B).

To be able to generalize these results to arrays with any NW topography, a theoretical model to predict the adhesion proximity was developed. Important for any theoretical model of adhesion proximity, one must take into consideration that the cell membrane is not penetrated by the NWs, but rather wrap the nanostructures in tight membrane invaginations.[13,21,22] Thus, a prediction of how a cell settles initially on various NW densities, loosely on top of the wires ("top") or tightly down to the bottom of the NW arrays ("bottom"), should consider the energy required to shape these membrane invaginations. For this purpose, it is useful to adopt a simple view of the cell as being a soft, elastic shell that is deformed by the NWs. The free energy (ΔG) of the adhering cell is then given by

$$\Delta G = -wA_c + \sigma\Delta O + \Delta G_b \quad (1)$$

where w is the specific adhesion energy, A_c is the surface contact area, σ is the surface tension, ΔO is the surface area

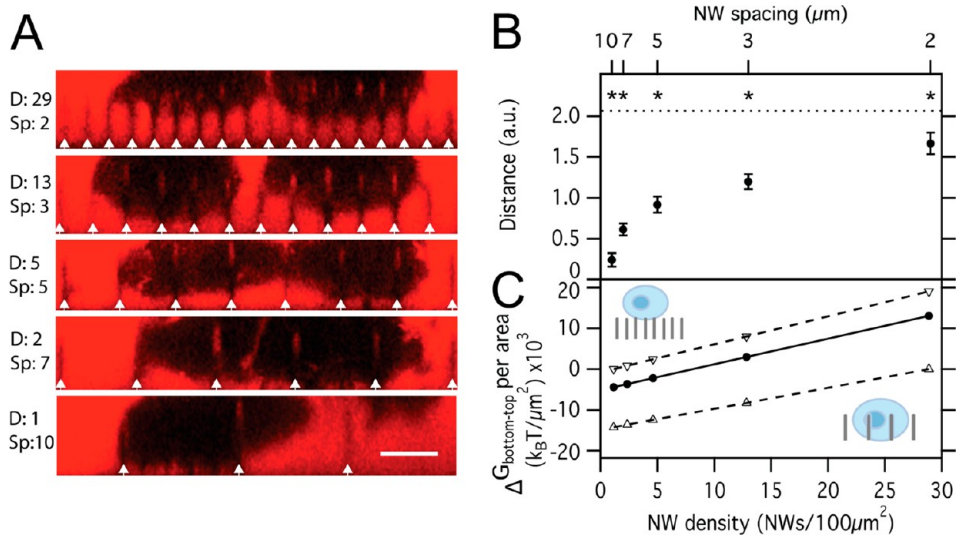

Figure 7. Tuning and predicting the density-dependent proximity between cells and nanowires (NWs). (A) Side-views of cells on NW arrays immersed in fluorescent medium show that living cells grow increasingly closer to the underlying chip surface as the NW density is decreased. D = density (NW/l00μm^2), Sp = spacing (μm). Scale bar = 5 μm. (B) This is supported by quantification of the distance between the cell and NW chip surface, where the values for all densities are significantly different from each other (∗). (C) This adhesion behavior can be predicted by a theoretical model, where it is demonstrated that it becomes energetically beneficial ($\Delta G_{bottom\text{-}top} < 0$) for cells to adhere close to the surface as the NW density is decreased. By input of values from the literature, it is predicted that cells should stay on top of the wires ($\Delta G_{bottom\text{-}top} > 0$) for the high-density arrays 13 and 29 NWs/100 μm^2 (=3 and 2 μm spacing), and settle all the way down to the support on the low-density arrays 1, 2, and 5 NWs/100μm^2 (=10, 7, and 5 μm spacing) (solid line). The theory predicts a shift between adhering on top or down to the chip surface as long as the specific adhesion energy (w) remains within the range of 3.4×10^{-18} J/μm^2 (dashed line above) to 6.3×10^{-17} J/μm^2 (dashed line below).

increase resulting from the transition from the spherical to the adhering shell, and ΔG_b is the elastic free energy associated with the bending of the soft shell.[35] Values for the constants w and σ, as well as the bending modulus κ which enters into ΔG_b (Supporting Information eqs S2 and S3), have to be measured for the given cell and surface. For a first prediction, the values $w = 2.2 \times 10^{-17}$J/μm^2,[36] $\sigma = 2.4 \times 10^{-17}$J/$\mu m^2$,[37] and $\kappa = 9 \times 10^{-19}$J[38] were used. This theoretical model suggests that it becomes energetically beneficial ($\Delta G_{bottom\text{-}top} < 0$) for cells to adhere close to the surface as the NW density is decreased (Figure 7C, Supporting Information eq S1). We find that, for the densities 1, 2, and 5 NWs/100 μm^2, it is predicted favorable for the cell to deform and adhere tightly to the NW array, whereas for the higher densities it is more likely that the cell floats on top of the array. $\Delta G_{bottom\text{-}top}$ is found to be relatively insensitive to changes in σ and very sensitive to changes in w and x (data not shown). As the exact value for w in this specific system is unknown, and since the theoretical model is very sensitive to changes in w, $\Delta G_{bottom\text{-}top}$ has also been plotted for $w = 3.4 \times 10^{-18}$ J/μm^2 and 6.3×10^{-17}J/μm^2 (Figure 7C). These values define the boundaries of the specific adhesion energy range, within which a shift between tight and loose adhesion is predicted in the investigated density range. Since a distinct and significant change in adhesion tightness is observed experimentally (Figure 7A, B), we expect the real value of w for our system to be within this range. In conclusion, the NW density affects the cell−surface adhesion proximity, which can be predicted by the energy cost of membrane deformation.

DISCUSSION

To aid the design of NW arrays for cellular applications, multidensity chips with geometrically controlled arrays of InAs NWs are utilized in this study to systematically investigate the effects of NW density on cellular health, adhesion, morphology, and division. In this study, the variability of cell-based data was taken into account by using samples of considerable size, and by only addressing statistical differences through the use of t tests.

Whereas the effect of NW diameter and length on cellular health and function has been addressed in several qualitative studies,[9,14,24,39] only a few studies have suggested an effect of NW density,[28,39] with only a single systematic study on ordered arrays.[9] Since even subtle changes in nanotopography can cause dramatic changes to the cell fate,[9,40,41] the need for homogenous arrays and systematic studies is emphasized, where each cell meets exactly the same topography every time. This is in contrast to previous studies on randomly positioned NWs with broad distributions of NW lengths, diameters, and spacings. For general applicability to other systems, the NW densities used here were chosen to cover the range of positioned and randomly placed NW, nanopillar, and nanotube spacings used in the community; from high-density ($\lesssim$ 2 μm spacing),[7−9,11,14,21,28,39,42,43] to mid-density ($\approx$5 μm spacing),[6,9,10,22,42,44−47] and to low-density ($\gtrsim$ 10 μm spacing)[44] NW arrays.

Using homogeneous multidensity NW chips, we consistently demonstrate that cell viability is not affected by the presence of InAs NWs in the wide range of densities tested. This is in line with reports from many other cell types and NW platforms,[10,14,48] and brings extended support for the suitability of NW arrays for cellular investigations. Other reports show that interfacing cells with certain NWs can have a negative impact on cell viability.[14,23] This discrepancy in observed cell health could be attributed to the specific cell type, NW material or NW geometry used in each study.

Over time, populations of cells are reduced,[24,49] maintained,[43,50] or expanded[6,39,42,47,51] when interfaced with NW arrays. Cell proliferation has previously been noted to occur on NWs.[28,52] By using techniques on both fixed and living cells, we demonstrate that cells are able to go through three key stages of

the cell cycle, S-phase, M-phase, and cytokinesis, while interfaced with NW chips. This is in line with results regarding cytokinesis on different nanotopographies and cell types.[53] Interestingly, we find that the number of cells in S-phase is increased by the presence of NWs, with a tendency to be increased on low density, as compared to high-density NW arrays. The discrepancy in results between this and the previous finding could be explained by the labeling of different epitopes, and thus different parts of the cell cycle. Possibly, the NWs influence the interfaced cells through an increased cell cycle synchronization, and/or prolonged S-phase dwell time, which fail to be revealed by a general investigation of overall cell proliferation rate.

Successful cell adhesion is a crucial feature in the design of NW array-based biosensors. Increased cellular adhesion on NWs compared to flat controls has been suggested previously.[15] By centrifugation forces, cells have been shown to adhere stronger to extremely dense Si NWs,[43] and migrate less on rings of vertical NWs.[48] Here we demonstrate that cells adhere stronger to NW arrays as compared to both InAs- and glass controls, and that the improved cell adhesion offered by NWs is independent on the density of the NWs in the range tested here. The reduced level of cell detachment on all densities compared to the controls cannot be explained by an increased surface contact area on NWs, since a calculation based on cell area and proximity to chip surface shows that even cells adhering to the tips of NWs, and thus having a low surface contact area, also adhere strongly to the NWs.

Low-aspect nanotopographies are known to affect FA formation and morphology.[18,40,54] Previously, arrays of high-aspect ratio Si NWs have been shown to promote expression of focal adhesion kinase,[43] whereas FAs were not visible in cells on ZnO nanorods.[23] On all densities we find FAs positioned both next to, and colocalized with NWs, without any preference for either. Interestingly though, we find the FA area to be significantly increased on NWs compared to especially glass control, and increased FA density and more elongated FAs in cells on NWs compared to InAs control. This response to the nanotopographies presented to the cells, especially by the high-density NW arrays, is suggested to contribute to the reported decreased levels of cell detachment from NWs, possibly in combination with the physical stabilization of cell membrane along the NWs provided by the actin cytoskeleton.

The morphology, and especially the area of the cell, will determine how many NWs each cell will contact on the NW array-based biosensor, and will thus be important to take into consideration when developing, for example, delivery platforms. NWs have been shown to enhance[55] or restrict[23−25] cell spreading, as well as maintain normal cell morphology.[6,16,39,48,50,56] In this study, we find that HEK293 cells are larger and more elongated on low-density NWs than on control and high-density NW arrays, both showing a tendency to decrease as the NW density increases. The same observation was made by Bucaro et al. on embryo-derived murine C3H10T1/2 cells using homogeneous NW arrays.[9] When the spacing between NWs increased from 2 to 4 μm spacing, the cell area tended to increase. However, the specific effect of NW density on cell morphology and size is most likely dependent both on the cell and NW array type, and should thus be investigated for each specific system of interest. As a side note, we find indications that the cell clustering is dependent on NW spacing, where cell clusters are smaller and tighter on high-density arrays, and larger clusters with increased cell−cell distance for low-density arrays. However, this still requires more investigation before firm conclusions can be drawn.

The tightness by which the cells adhere to the NW array is decisive of the electrical seal and signal strength achieved in NW-based electrophysiology.[6,7,21] We systematically show that the NW density is an important factor for the proximity between the living cells and the NW arrays. This knowledge can be directly applied to electrophysiological model systems with HEK293 cells,[7] to possibly improve the electrical seal and signal-to-noise ratio even further by increasing the spacing between the NW electrodes. Furthermore, we suggest a theoretical model to predict the initial adhesion proximity. This model does not take into account the forces involved in displacing of cellular contents, which may be a fair assumption for very thin structures, such as NWs, but probably means that the validity of the model decreases if the diameter of the vertical structures is increased, or when going to very high NW densities. Another model explains the density-dependent shift from floating cells to the more intimately adhering cells with the existence of a critical distance above which the cell cannot reach between neighboring NWs, and thus settle down on the surface of the NW array.[9] The NW spacing is only considered in our theory as a density, but it may well be important in itself, especially when it approaches the size of the cell. The previous model, however, does not take into account that the cell membrane adapts dramatically to the NWs as it sinks into the array. Thus, the two theories may be complementary, rather than mutually exclusive, and can predict the NW density appropriate for achieving the desired adhesion tightness for NW-based biosensors.

The NW-induced cellular responses could be speculated to be the outcome of modified gene expression; either indirectly through the remodeled FA signaling complexes, or as a direct effect of the increased NW-induced nuclear membrane curvature, which in turn affects the proximity between chromosomes and the nuclear membrane and can lead to altered gene expression.[57]

To single out and study the impact of NWs per se, control surfaces of the same material and roughness as the "flat" area between NWs (Figure S1, Supporting Information) is here suggested to be a superior choice over previously used planar, polished, or atomically flat material.[9,11,15,23,24,28,43] Thus, in our study, both glass coverslip and nonpolished InAs were used as controls. Interestingly, for some parameters, such as the cell area and detachment level, the two control surfaces gave different results. This further emphasizes the importance of carefully choosing the appropriate control for each experiment.

Using state-of-the-art multidensity chips, we show that the presence of NWs increases the number of S-phase cells and upregulates FA formation, without affecting cell viability. Importantly, a systematic tuning of NW density affects several cellular parameters, such as cell morphology and adhesion proximity, and will thus be instrumental to take into consideration when optimizing NW-based biosensors for cellular applications.

■ ASSOCIATED CONTENT

Ⓢ Supporting Information

Detailed description of InAs nanowire fabrication, demonstration of the validity of the InAs control surface (Figure S1), a movie demonstrating cell adhesion, division and dynamics on NW array (Movie S1), the actin cytoskeleton in HEK293 cell on glass control (Figure S3), focal adhesion formation on low-

density NW array (Figure S4), and a full description of the theoretical model of adhesion proximity, including eqs S1−S3. This material is available free of charge via the Internet at http://pubs.acs.org.

AUTHOR INFORMATION

Notes

The authors declare no competing financial interest.

ACKNOWLEDGMENTS

The authors thank Peter Fuerst, Peter Krogstrup, and Claus B. Sørensen for fruitful discussions. For financial support, we thank the Danish Agency for Science Technology and Innovation (The Danish Council for Strategic Research - CLIPS and ANaCell projects, and The Danish Natural Science Research Council − FTP 11-116984), UNIK Synthetic Biology (funded by the Danish Ministry for Science, Technology and Innovation), and French research grants from Region Alsace and La Ligue contre le cancer CCIR-FE. We thank Danish Fundamental Metrology (DFM) for the AFM measurements.

REFERENCES

(1) Alivisatos, A. P.; Andrews, A. M.; Boyden, E. S.; Chun, M.; Church, G. M.; Deisseroth, K.; Donoghue, J. P.; Fraser, S. E.; Lippincott-Schwartz, J.; Looger, L. L.; Masmanidis, S.; McEuen, P. L.; Nurmikko, A. V.; Park, H.; Peterka, D. S.; Reid, C.; Roukes, M. L.; Scherer, A.; Schnitzer, M.; Sejnowski, T. J.; Shepard, K. L.; Tsao, D.; Turrigiano, G.; Weiss, P. S.; Xu, C.; Yuste, R.; Zhuang, X. *ACS Nano* **2013**, *7*, 1850−1866.
(2) Ilie, I.; Ilie, R.; Mocan, T.; Bartos, D.; Mocan, L. *Int. J. Nanomed.* **2012**, *7*, 2211−2225.
(3) He, Y.; Fan, C. H.; Lee, S. T. *Nano Today* **2010**, *5*, 282−295.
(4) Berthing, T.; Sørensen, C. B.; Nygård, J.; Martinez, K. L. *J. Nanoneurosci.* **2009**, *1*, 3−9.
(5) VanDersarl, J. J.; Xu, A. M.; Melosh, N. A. *Nano Lett.* **2012**, *12*, 3881−3886.
(6) Xie, C.; Lin, Z.; Hanson, L.; Cui, Y.; Cui, B. *Nat. Nanotechnol.* **2012**, *7*, 185−190.
(7) Robinson, J. T.; Jorgolli, M.; Shalek, A. K.; Yoon, M. H.; Gertner, R. S.; Park, H. *Nat. Nanotechnol.* **2012**, *7*, 180−184.
(8) Na, Y. R.; Kim, S. Y.; Gaublomme, J. T.; Shalek, A. K.; Jorgolli, M.; Park, H.; Yang, E. G. *Nano Lett.* **2013**, *13*, 153−158.
(9) Bucaro, M. A.; Vasquez, Y.; Hatton, B. D.; Aizenberg, J. *ACS Nano* **2012**, *6*, 6222−6230.
(10) McKnight, T. E.; Melechko, A. V.; Griffin, G. D.; Guillorn, M. A.; Merkulov, V. I.; Serna, F.; Hensley, D. K.; Doktycz, M. J.; Lowndes, D. H.; Simpson, M. L. *Nanotechnology* **2003**, *14*, 551−556.
(11) Berthing, T.; Bonde, S.; Sørensen, C. B.; Utko, P.; Nygård, J.; Martinez, K. L. *Small* **2011**, *7*, 640−647.
(12) Persson, H.; Beech, J.; Samuelson, L.; Oredsson, S.; Prinz, C.; Tegenfeldt, J. *Nano Res.* **2012**, *5*, 190−198.
(13) Mumm, F.; Beckwith, K. M.; Bonde, S.; Martinez, K. L.; Sikorski, P. *Small* **2013**, *9*, 263−272.
(14) Kim, W.; Ng, J. K.; Kunitake, M. E.; Conklin, B. R.; Yang, P. *J. Am. Chem. Soc* **2007**, *129*, 7228−7229.
(15) Hällström, W.; Mårtensson, T.; Prinz, C. N.; Gustavsson, P.; Montelius, L.; Samuelson, L.; Kanje, M. *Nano Lett.* **2007**, *7*, 2960−2965.
(16) Shalek, A. K.; Robinson, J. T.; Karp, E. S.; Lee, J. S.; Ahn, D.-R.; Yoon, M.-H.; Sutton, A.; Jorgolli, M.; Gertner, R. S.; Gujral, T. S.; Macbeath, G.; Yang, E. G.; Park, H. *Proc. Natl. Acad. Sci. U.S.A.* **2010**, *107*, 1870−1875.
(17) Petit, V.; Thiery, J. P. *Biol. Cell* **2000**, *92*, 477−494.
(18) Geiger, B.; Spatz, J. P.; Bershadsky, A. D. *Nat. Rev. Mol. Cell Biol.* **2009**, *10*, 21−33.
(19) Gardel, M. L.; Schneider, I. C.; Aratyn-Schaus, Y.; Waterman, C. M. *Annu. Rev. Cell Dev. Biol.* **2010**, *26*, 315−333.
(20) Prinz, C.; Hallstrom, W.; Martensson, T.; Samuelson, L.; Montelius, L.; Kanje, M. *Nanotechnology* **2008**, *19*, 345101.
(21) Hanson, L.; Lin, Z. C.; Xie, C.; Cui, Y.; Cui, B. *Nano Lett.* **2012**, *12*, 5815−5820.
(22) Berthing, T.; Bonde, S.; Rostgaard, K. R.; Madsen, M. H.; Sørensen, C. B.; Nygård, J.; Martinez, K. L. *Nanotechnology* **2012**, *23*, 415102.
(23) Lee, J.; Kang, B. S.; Hicks, B.; Chancellor, T. F., Jr.; Chu, B. H.; Wang, H.-T.; Keselowsky, B. G.; Ren, F.; Lele, T. P. *Biomaterials* **2008**, *29*, 3743−3749.
(24) Kuo, S. W.; Lin, H. I.; Ho, J. H.; Shih, Y. R.; Chen, H. F.; Yen, T. J.; Lee, O. K. *Biomaterials* **2012**, *33*, 5013−5022.
(25) Kim, D. J.; Lee, G.; Kim, G. S.; Lee, S. K. *Nanoscale Res. Lett.* **2012**, *7*, 637.
(26) Li, Z.; Song, J.; Mantini, G.; Lu, M. Y.; Fang, H.; Falconi, C.; Chen, L. J.; Wang, Z. L. *Nano Lett.* **2009**, *9*, 3575−3580.
(27) Golias, C. H.; Charalabopoulos, A.; Charalabopoulos, K. *Int. J. Clin. Pract.* **2004**, *58*, 1134−1141.
(28) Piret, G.; Perez, M. T.; Prinz, C. N. *Biomaterials* **2013**, *34*, 875−887.
(29) Kim, M.; An, S. M.; Koh, J. S.; Jang, D. I.; Boo, Y. C. *J. Cosmet. Sci.* **2011**, *62*, 515−523.
(30) Thomas, P.; Smart, T. G. *J Pharmacol. Toxicol. Methods* **2005**, *51*, 187−200.
(31) Madsen, M. H.; Krogstrup, P.; Johnson, E.; Venkatesan, S.; Mühlbauer, E.; Scheu, C.; Sørensen, C. B.; Nygård, J. *J. Cryst. Growth* **2013**, *364*, 16−22.
(32) Abankwa, D.; Vogel, H. *J. Cell Sci.* **2007**, *120*, 2953−2962.
(33) Huang, Q.; Cheng, A.; Antensteiner, M.; Lin, C.; Vogler, E. A. *Biomaterials* **2013**, *34*, 434−441.
(34) Gratzner, H. G. *Science* **1982**, *218*, 474−475.
(35) Sackmann, E.; Bruinsma, R. F. *ChemPhysChem* **2002**, *3*, 262−269.
(36) Simson, R.; Wallraff, E.; Faix, J.; Niewohner, J.; Gerisch, G.; Sackmann, E. *Biophys. J.* **1998**, *74*, 514−522.
(37) Needham, D.; Hochmuth, R. M. *Biophys. J.* **1992**, *61*, 1664−1670.
(38) Khatibzadeh, N.; Gupta, S.; Farrell, B.; Brownell, W. E.; Anvari, B. *Soft Matter* **2012**, *8*, 8350−8360.
(39) Shalek, A. K.; Gaublomme, J. T.; Wang, L.; Yosef, N.; Chevrier, N.; Andersen, M. S.; Robinson, J. T.; Pochet, N.; Neuberg, D.; Gertner, R. S.; Amit, I.; Brown, J. R.; Hacohen, N.; Regev, A.; Wu, C. J.; Park, H. *Nano Lett.* **2012**, *12*, 6498−6504.
(40) Dalby, M. J.; Riehle, M. O.; Johnstone, H. J.; Affrossman, S.; Curtis, A. S. *Tissue Eng.* **2002**, *8*, 1099−108.
(41) Cavalcanti-Adam, E. A.; Volberg, T.; Micoulet, A.; Kessler, H.; Geiger, B.; Spatz, J. P. *Biophys. J.* **2007**, *92*, 2964−2974.
(42) Denoual, M.; Chiral, M.; LePioufle, B. *Nanobiotechnology* **2005**, *1*, 389−394.
(43) Qi, S.; Yi, C.; Ji, S.; Fong, C.-C.; Yang, M. *ACS Appl. Mater. Interfaces* **2009**, *1*, 30−34.
(44) Mann, D. G. J.; McKnight, T. E.; McPherson, J. T.; Hoyt, P. R.; Melechko, A. V.; Simpson, M. L.; Sayler, G. S. *ACS Nano* **2008**, *2*, 69−76.
(45) McKnight, T. E.; Melechko, A. V.; Fletcher, B. L.; Jones, S. W.; Hensley, D. K.; Peckys, D. B.; Griffin, G. D.; Simpson, M. L.; Ericson, M. N. *J. Phys. Chem. B* **2006**, *110*, 15317−15327.
(46) McKnight, T. E.; Melechko, A. V.; Hensley, D. K.; Mann, D. G.; Griffin, G. D.; Simpson, M. L. *Nano Lett.* **2004**, *4*, 1213−1219.
(47) Peer, E.; Artzy-Schnirman, A.; Gepstein, L.; Sivan, U. *ACS Nano* **2012**, *6*, 4940−4946.
(48) Xie, C.; Hanson, L.; Xie, W.; Lin, Z.; Cui, B.; Cui, Y. *Nano Lett.* **2010**, *10*, 4020−4024.
(49) Zaveri, T. D.; Dolgova, N. V.; Chu, B. H.; Lee, J.; Wong, J.; Lele, T. P.; Ren, F.; Keselowsky, B. G. *Biomaterials* **2010**, *31*, 2999−3007.
(50) Ciofani, G.; Genchi, G. G.; Mattoli, V. *Mater. Sci. Eng. C* **2012**, *32*, 341−347.
(51) Zhou, J.; Li, B.; Lu, S.; Zhang, L.; Han, Y. *ACS Appl. Mater. Interfaces* **2013**, *5*, 5358−5365.

(52) Persson, H.; Kobler, C.; Molhave, K.; Samuelson, L.; Tegenfeldt, J. O.; Oredsson, S.; Prinz, C. N. *Small* **2013**, DOI: 10.1002/smll.201300644.
(53) Albuschies, J.; Vogel, V. *Sci. Rep.* **2013**, *3*, 1658.
(54) Biggs, M. J. P.; Richards, R. J.; Dalby, M. J. *Nanomed.: Nanotechnol., Biol., Med.* **2010**, *6*, 619−633.
(55) Abdul Kafi, M.; El-Said, W. A.; Kim, T. H.; Choi, J. W. *Biomaterials* **2012**, *33*, 731−739.
(56) Park, S.; Kim, Y.-S.; Kim, W. B.; Jon, S. *Nano Lett.* **2009**, *9*, 1325−1329.
(57) Finlan, L. E.; Sproul, D.; Thomson, I.; Boyle, S.; Kerr, E.; Perry, P.; Ylstra, B.; Chubb, J. R.; Bickmore, W. A. *PLoS Genet.* **2008**, *4*, e1000039.